PNAS RESEARCH ARTICLE | PHYSICS

Clever algorithms for glasses work by time reparameterization

Federico Ghimenti[a,b,1], Ludovic Berthier[c,d], Jorge Kurchan[e], and Frédéric van Wijland[b]

Affiliations are included on p. 8.

Edited by Andrea Liu, University of Pennsylvania, Philadelphia, PA; received July 31, 2025; accepted December 19, 2025

The ultraslow dynamics of glass-formers has been explained by two views often considered as mutually exclusive: One invokes locally hindered mobility, and the other rests on the complexity of the configuration space. Here, we show that time evolution responds strongly to details of the dynamics by changing the speed of time flow: It has time-reparameterization softness. This finding reconciles both views: While local constraints reparameterize the flow of time, the global landscape determines relationships between different correlations at the same times. We show that modern algorithms developed to accelerate the relaxation to equilibrium act by changing the time reparameterization. Their success thus relies on their ability to exploit reparameterization softness. We conjecture that these results extend beyond the realm of glasses to the optimization of more general constraint satisfaction problems and to broader classes of algorithms.

glasses | sampling algorithms | time reparameterization

Significance

Why do amorphous materials flow so slowly when temperature or density is mildly changed? Competing explanations typically fall into two pictures, where the dynamics is either controlled by the static structure of the energy landscape or hindered by constraints of kinetic origin. This debate was recently fueled by the observation that modern computer algorithms can explore the same static landscape at a much faster pace. Here, we reconcile both viewpoints using the concept of time reparameterization. We show that modern algorithms reparameterize the time at which glassy dynamics unfolds. As a result, kinetic constraints determine the choice of reparameterization, while the static landscape fully determines the dynamic bottlenecks. Both views thus contain an essential element of truth.

In contrast to many fields of physics, acceptable microscopic models of glasses are easy to construct: Hard spheres are a good example and may be readily simulated or studied experimentally (1). Theoretical efforts have instead been mostly directed at finding the right questions to ask (2). Phenomenological arguments abound and are constantly being refined, while exact analytical results are rare, a recent notable exception being the case of particles living in an infinite-dimensional space (3, 4).

Several ideas have been proposed to capture the origin of the dramatic slowdown of the dynamics as density is increased or as temperature is lowered. These have been classified into two families. On the one hand, there is a landscape paradigm, where the energy function and associated static expectation values encode for the dynamical behavior (5–10). A dynamic transition, where the relaxation time diverges at a finite temperature, is then only possible if there exists an underlying, thermodynamic and landscape-based, one (11–16). On the other hand stands the view that glassiness is dynamical in essence. An example is when local rearrangements, and hence flow, are dominated by dynamic facilitation (17, 18). This occurs when localized, mobile regions diffusing through the system are essentially noninteracting and cannot be born or die except by branching and coalescing, a mechanism absent from the high-dimensional solution (19, 20).

The latter view and the statics-dynamics debate were recently boosted by the development of numerical algorithms that drastically accelerate the dynamical evolution (21–23), while preserving the Boltzmann distribution. In particular, the outstanding performance of the swap Monte Carlo algorithm has been interpreted as indicating that the energy landscape paradigm is insufficient to account for glassiness and thus as a sign that real glasses behave as models with local kinetic constraints (19, 24, 25).

Our central finding is that both pictures are simultaneously right. That there is no contradiction between them is the consequence of a remarkable property, time reparameterization invariance, that is asymptotically exact—i.e., if and when the dynamics are slow—in the mean-field theory of aging in disordered systems (26–29). For realistic, finite-dimensional models, we are at present far from being able to prove analytically that time reparameterization invariance holds. Instead, we may seek whether the associated time reparameterization softness (30–34) is observed in them. If true, this implies that the flow of time can be modified with weak perturbations, exactly like a film being projected using an old hand-cranked projector, where the operator can effortlessly modify the speed of the projection but has no control over the film's content. Physically, this implies that local particle rearrangements and short-time relaxation can be different depending on the specific dynamics and algorithm employed. Each algorithm yields its own collective relaxation time, but they trace the same trajectory in configuration space as the system slowly and collectively relaxes. This description echoes earlier attempts to remove time from the description of relaxation phenomena (35–38). Overall, our results

Author contributions: F.G., L.B., J.K., and F.v.W. designed research; F.G., L.B., J.K., and F.v.W. performed research; F.G., L.B., J.K., and F.v.W. analyzed data; and F.G., L.B., and F.v.W. wrote the paper.

The authors declare no competing interest.

This article is a PNAS Direct Submission.

[1]To whom correspondence may be addressed. Email: ghimenti@stanford.edu.

This article contains supporting information online at https://www.pnas.org/lookup/suppl/doi:10.1073/pnas.2520818123/-/DCSupplemental.

Published January 23, 2026.

provide a clear means of sieving out the energy-landscape-dependent features from purely dynamical ones.

Our presentation begins with numerical and analytical observations of parametric plots of correlations in glass-formers endowed with vastly different time evolutions but sharing the same stationary Boltzmann distribution. The spectacular impact of reparameterizations calls for theoretical support that we address with an exact solution in mean field and eventually by describing a general picture with consequences well beyond the physics of glasses.

The Proof Is in the Pudding

Parametric Plot of Time Correlations. As glassiness sets in, the decay of time correlations follows a two-step scenario beginning with a fast relaxation, followed by a slow decay that extends up to a characteristic time τ_α. We track the relaxation of the system in terms of a real space, collective overlap function F_o, defined by

$$F_o(a,t) \equiv \frac{1}{N}\sum_{i,j}\langle\theta\left(a-|\mathbf{r}_i(t)-\mathbf{r}_j(0)-\Delta\mathbf{r}_{\rm com}(t)|\right)\rangle, \quad [1]$$

where $\Delta\mathbf{r}_{\rm com}(t)$ is the displacement of the center of mass of the system, and θ is the step function. Physically, the function F_o compares the density fields of the system between times 0 and t. The angular brackets represent an average over the Boltzmann initial state and over time realizations of the dynamics. The parameter a, chosen to be smaller than any particle's diameter, selects the scale over which the relaxation is monitored. This is better suited than the usual self-intermediate scattering function [see *SI Appendix*, sections 1 and 3] for discussing various algorithms on equal footing. In practice, we plot a connected and normalized overlap function $Q_o(a,t)=(F_o-q_r)/(1-q_r)$, with $q_r=\frac{4\pi}{3}\rho_0 a^3$ in three dimensions, and ρ_0 the density of the system. This function decays to 0 at large times for any value of a and is normalized to unity at $t=0$. The statements we make concern the late stages of the relaxation process near τ_α.

When the goal is to sample the Boltzmann distribution, the algorithm being used does not need to respect actual physical constraints. For instance, introducing particle swaps with detailed balance, while clearly unphysical, has been shown to drastically reduce τ_α. Other proposals rely on irreversible methods that affect translation moves and/or particle swaps. The overall two-step relaxation shape of $Q_o(a,t)$ is also found in these vastly different dynamical evolutions. Our central result, sketched in Fig. 1, is that all dynamics, fast and slow, encapsulate the same physical evolution of the correlations. To test time reparameterization softness, we eliminate time in parametric plots of $Q_o(a,t)$ for two values of a and for various dynamics in different systems with glassy behavior. The collapse of the curves then directly expresses time-reparameterization invariance. Our conjecture is that this collapse occurs whenever both the algorithms display slow relaxation, with long lived plateaus of the same height in the decay of their dynamical correlation functions. The numerical evidence supporting these claims is our main result.

Irreversible Translation Moves. We begin with a three-dimensional binary Kob–Andersen mixture (39) evolving through an overdamped Langevin process. The convergence of this dynamics to the same Boltzmann distribution can be accelerated by exerting on every particle an extra force transverse to its local energy gradient (40–42). We use the dimensionless parameter γ to quantify the relative strength of transverse to radial forces: the larger γ, the greater the speed-up (see *Materials and Methods* for further details).

We numerically integrate the dynamics at a low temperature $T=0.48$, where the relaxation spans several orders of magnitude. In Fig. 2 *A* and *B* we plot the time evolution of Q_o, evaluated at two distinct lengths a_1, a_2. In the presence of transverse forces, the relaxation of the system is faster compared with the equilibrium dynamics by a factor ≈ 4 for $\gamma=4$ and by a factor ≈ 7 for $\gamma=10$. Both dynamics exhibit signs of two-step relaxation, and in the late part of the relaxation the shape of the curves is very similar, even when passing from $\gamma=0$ to $\gamma=10$. In Fig. 2*C*, we represent $Q_o(a_1,t)$ as a function of $Q_o(a_2,t)$ in a parametric plot, for $\gamma=0,4$, and 10. Their collapse shows that there exists a reparameterization of time such that the slow relaxation of the system with transverse forces coincides with the slow relaxation of the system under equilibrium dynamics: transverse forces speed up the slow dynamics of the system by means of a time reparameterization. Recent results (40–42) demonstrated that at low temperatures the dynamic pathways involve genuine nonequilibrium currents. Yet, these dynamic pathways display time reparameterization.

We have also compared the dynamics of polydisperse hard spheres with the equilibrium Metropolis Monte Carlo algorithm against the irreversible Event Chain Monte Carlo (43): a protocol of driven and collective rejection-free displacements of chains of particles which are microscopically very different from the local moves of the Metropolis Monte Carlo algorithm. We discovered that Event Chain also operates in glassy dynamics by reparameterizing the time over which the long-time relaxation occurs. The numerical data supporting this statement are shown in *SI Appendix*, section 2.

Swap Monte Carlo Algorithm. We push our exploration of time reparameterization invariance by probing the Swap Monte Carlo algorithm (21) (hereafter denoted as "Swap"). Swap implements reversible exchanges of diameters between pairs of particles. For continuously polydisperse hard-spheres, this allows the particle diameters to fluctuate, potentially opening up additional relaxation channels (20, 44–46) that can speed up the dynamics by several orders of magnitude (22, 47). However, we claim that in the region where the dynamics is slow for both Metropolis and Swap algorithms, the acceleration achieved by Swap results again from a reparameterization of time with respect to the local Metropolis dynamics.

To see this, we compare Metropolis and Swap dynamics in a dense system of continuously polydisperse hard spheres. We tune the rate of swaps p_s to work in a regime where the speedup provided by Swap encompasses about four orders of magnitude, and track the relaxation by means of the overlap function $Q_o(a,t)$. In Fig. 3 *A–C*, we show the time evolution of $Q_o(a,t)$ for three different values of a. For Metropolis dynamics, the decay of Q_o covers several orders of magnitude, with signs of a two-step relaxation showing up for the lowest value of a. Turning on the swap moves, the curves depart from the ones obtained with the Metropolis dynamics, and their decay is faster.

In Fig. 3 *D–F*, we show parametric plots of $Q_o(a_i,t)$ as a function of $Q_o(a_j,t)$ for all possible combinations (a_i,a_j) of distinct parameters for the overlap function. All the curves for the dynamics with different swap probabilities nearly collapse on top of each other, and the four-order of magnitude speed up disappears, suggesting that even an algorithm as powerful as Swap works by reparameterizing time. We have observed that the quality of the collapse improves when density is increased and

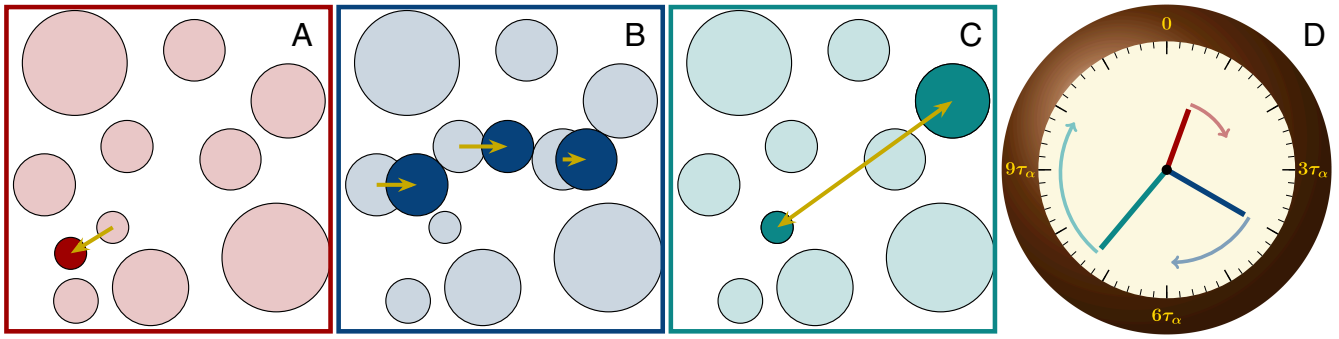

Fig. 1. Sketch of three algorithms performing dramatically different moves on the same system: (*A*) local equilibrium translations; (*B*) directed displacement of chains of particles; (*C*) exchange of particle diameters. (*D*) The effect of these moves can be encapsulated into a change of the pace at which the clock of the system is ticking. This is time reparameterization softness.

all curves display enhanced sign of two-step decay, suggesting even better collapse could be observed if we could simulate longer timescales. We expect that the time window over which data collapse is observed increases when the average relaxation becomes larger, an observation that would deserve further work.

Irreversible versions of Swap have recently been proposed (48, 49) that further accelerate the dynamics by performing driven, collective exchanges of particle diameters. The results are as above, see *SI Appendix*, sections 5 for data supporting our findings.

Kinetically Constrained Model. We now provide an instance of glassy dynamics that does not display time reparameterization softness because it is controlled by purely local constraints. We study the dynamics of the soft-East kinetically constrained model introducing an analog of swap moves, as proposed in ref. 24. Without softness, the original East model consists of N binary variables $n_i \in \{0, 1\}$ on a one-dimensional periodic lattice. Sites with $n_i = 1$ are occupied by an excitation. In the spirit of local defects in crystal, excitations represent regions where structural rearrangement can take place, transitioning from $n_i = 1$ to $n_i = 0$. The thermodynamic properties are trivial and are governed by the temperature T and the energy cost J of an excitation. The relaxation is hindered by kinetic constraints: the reversible creation and destruction of an excitation can take place only on a site immediately to the right of an excitation, thus incorporating dynamical facilitation.

In the soft version, each site is supplemented with a binary softness parameter, which modifies the kinetic constraint, allowing for the birth and death of isolated excitations. Spontaneous updates of the softness are controlled by a swap-like process with rate r_s. When $r_s = 0$, only the softness of already existing excitations can change. For $r_s \neq 0$, the softness of any site can be updated (see *Materials and Methods* for more details). By changing r_s we can thus speed the dynamics up and investigate whether time reparameterization is at work in the system.

We simulate the dynamics of the soft-East model with swap updates. For a fixed temperature we change the softness update rate from $r_s = 0$ to large values. We track the relaxation of the system using the persistence function $P(t)$, which measures the fraction of spins that have not yet flipped up to time t, and is thus analogous to the overlap function used for structural glasses. The evolution of $P(t)$ with r_s is shown in Fig. 4*A*. The persistence function starts from 1 when no spin has flipped and decays to 0 when all spins have been updated at least once. The behavior of $P(t)$ at short times does not change upon varying r_s. At later times, the curves for $r_s \neq 0$ depart from the curve obtained for $r_s = 0$, achieving a speedup of almost three orders of magnitude for the largest r_s. We also looked at the time autocorrelation of the spins, $C_n(t)$, see Fig. 4*B*. For any swap rate r_s, the decay of $C_n(t)$ is about an order of magnitude faster than the decay of the corresponding persistence curve $P(t)$, but the overall behavior is very similar.

The long time decay of $P(t)$ and $C_n(t)$ have different shapes when r_s changes. In Fig. 4*C* we show parametric plots of $C_n(t)$ against $P(t)$. The different curves do not collapse, even for the lowest r_s value. Differently from the particle models, the correlation functions studied in Fig. 4 are single spin functions, as collective correlations vanish for this model. To assess whether the access to nonvanishing collective correlations on different lengthscales can restore time-reparameterization invariance, we investigate in *SI Appendix*, sections 6 a different

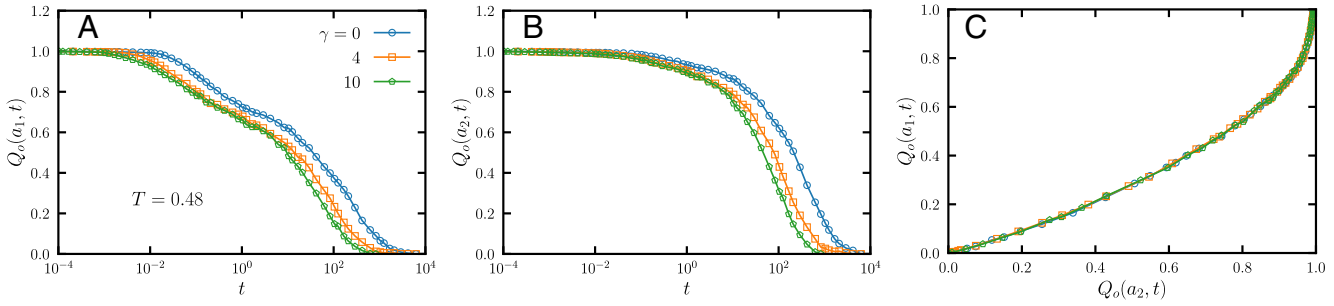

Fig. 2. (*A* and *B*) Time evolution of the overlap function $Q_o(a, t)$ for a Kob–Andersen mixture under equilibrium overdamped Langevin dynamics ($\gamma = 0$) and with transverse forces ($\gamma = 4$ and $\gamma = 10$), for $a_1 = 0.2d_{AA}$ and $a_2 = 0.3d_{AA}$. (*C*) Time reparameterization invariant plot, obtained representing $Q_o(a_1, t)$ as a function of $Q_o(a_2, t)$.

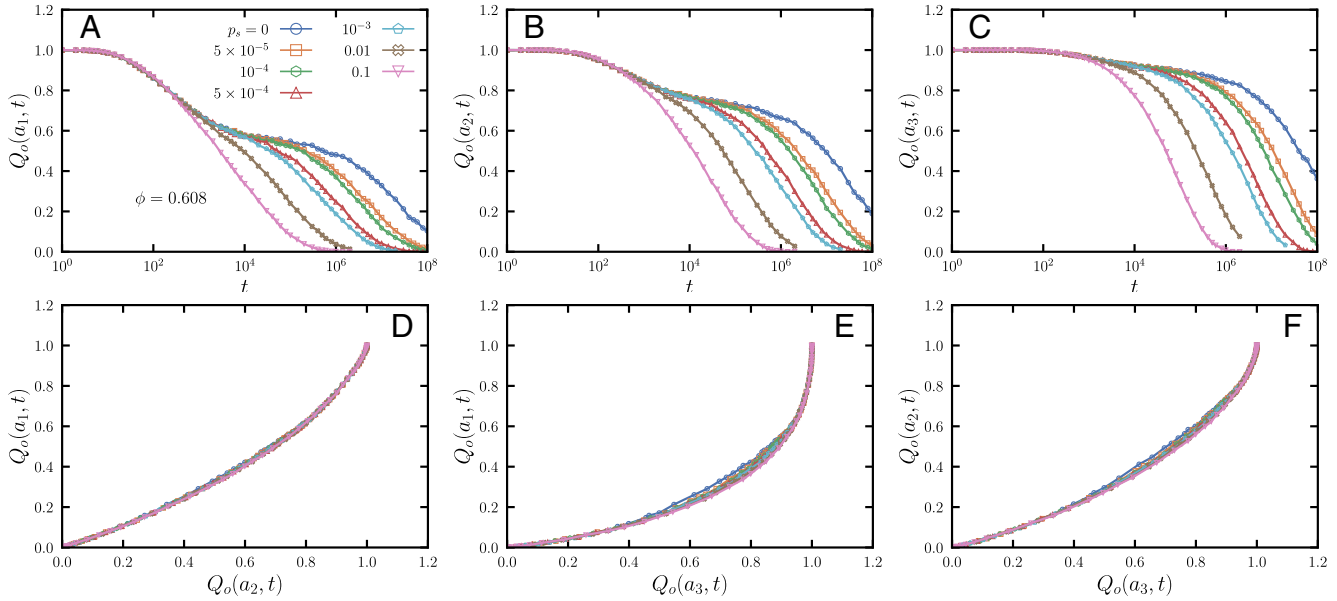

Fig. 3. (*A–C*) Time evolution of the collective overlap function in continuously polydisperse hard spheres using Metropolis algorithm ($p_S = 0$) and Swap Monte Carlo with different swap probabilities at fixed packing fraction $\phi \equiv \rho_0 \frac{\pi}{6} \overline{d^3}$. In each panel, a different value of a is used. $a_1 = 0.15\overline{d}$, $a_2 = 0.2\overline{d}$, $a_3 = 0.3\overline{d}$. (*D–F*) Parametric plots of $Q_o(a_i, t)$ as a function of $Q_o(a_j, t)$.

kinetically constrained model with softness updates where collective correlations can be studied. We do not see a collapse in the parametric plots in that system either. The acceleration provided by the additional updates of the softness are not simply described by reparameterization of time. This also shows that the reparameterization-invariant data collapse observed in finite dimensional particle models is not trivial.

Time Reparameterization Softness. Mean-field glass models provide a tractable case (or limit, in the case of large dimensionality) where there is analytic support to the concept of time reparameterization. We first describe how time reparameterization softness generally arises in mean-field frameworks, and then tackle analytically a specific mean-field model.

Glasses primarily respond to external perturbations by changing the pace of their evolution, like the same movie projected at various speeds. Consider a correlation function obtained by measuring a quantity at two times and repeating the experiment many times under statistically equal conditions, $C_A(t, t') = \langle A(t)A(t')\rangle$. (Averages are over independent experiments). Alternatively, we may apply an infinitesimal pulse field changing the Hamiltonian to $H(t) \to H + hA\delta(t - t')$ at time t' and measure the change in the expectation at time t at linear order, $R_A(t, t') = \frac{\delta\langle A(t)\rangle}{\delta h}$. In equilibrium, the response and correlation functions are linearly related by the fluctuation–dissipation theorem, $TR_A(t - t') = -\partial_t C_A(t - t')$, with T the temperature of the system.

In mean-field models, given a set of observables A_α, it is possible to write closed exact equations for pairs of response-correlation functions C_{A_α} and R_{A_α}, valid in and out of equilibrium, which do not have any explicit time dependence. If the relaxation of the system is very slow, one may neglect the time-derivatives and solve for all the C_{A_α}, R_{A_α}. The solution holds however up to a time reparameterization: if $\{R_{A_\alpha}(t, t'), C_{A_\alpha}(t, t')\}$ is a solution, then $\{R_{A_\alpha}(h(t), h(t'))\frac{\mathrm{d}h}{\mathrm{d}t'}, C_{A_\alpha}(h(t), h(t'))\}$ is also a solution. The function $h(t)$ is smooth and increasing, and it encodes the adopted reparameterization of time.

The true solution, where the time derivative is not neglected, is unique, and hence only one of the $h(t)$ constitutes the "good" parameterization. However, other reparameterizations can be selected, for instance in the presence of an applied shear (50), or during jump events (34) between distant configurations at low energy, and can be made visible when looking at fluctuations of the correlation-response curves (27–29).

By making a parametric plot of any one of the $\{R_{A_\alpha}(t, t'), C_{A_\alpha}(t, t')\}$ in terms of a single, reference correlation

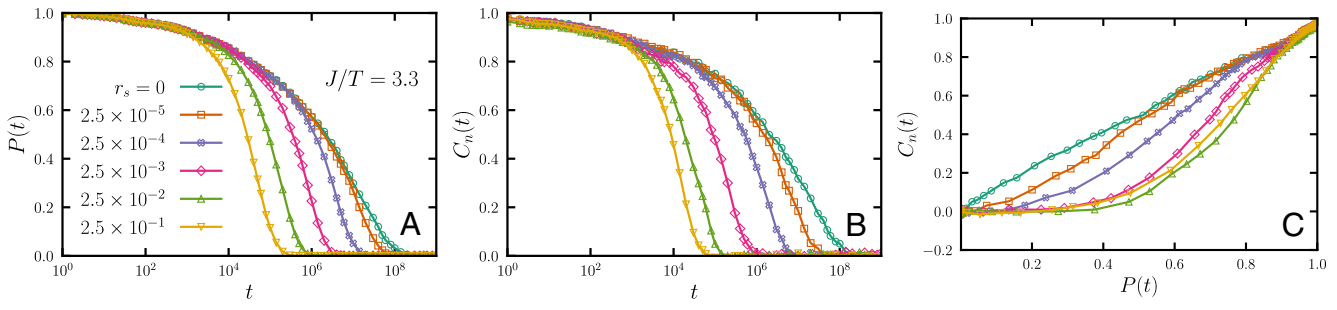

Fig. 4. Dynamics of a soft-East kinetically constrained model with softness updates, using different values of the softness updated rate r_S. (*A*) persistence function as a function of time for different swap rates. (*B*) Time decay of the spin–spin autocorrelation function C_n. (*C*) Parametric plot of C_n against P. The absence of collapse in (*C*) reveals the lack of time reparameterization invariance.

$C_o(t,t')$, we obtain a single master curve independent of the chosen time reparameterization (51). In this representation, we are measuring everything in terms of a "clock" $C_o(t,t')$, which determines the "material time" (35, 36, 38, 52).

The concept of time reparameterization first arose in the context of dynamic mean-field theory of aging systems (53). As discussed here and in the specific mean-field model solved below, it generalizes to mean-field models in a wide range of situations, and it appears as a generic property of mean-field glasses in a slow dynamical regime. The numerical results provided in this work demonstrate that its domain of applicability is not restricted to mean-field models, but is an observed property of realistic, finite dimensional glass models. This is reminiscent of the idea of an effective temperature (54) that first emerged from the analytic solution of the aging dynamics of a mean-field spin glass model (53). Along the years, the existence of effective temperatures was then demonstrated in a much wider range of finite dimensional situations (55).

A Solvable Model. The above general discussion can be illustrated on an explicit example. We consider the mean-field p-spin glass model, which is driven out of equilibrium while respecting the Boltzmann distribution. To do so, we couple two copies of the system by means of a nonreciprocal force chosen to preserve the factorized Boltzmann distributions for the two systems (56). As for transverse forces, a dimensionless parameter γ controls the relative strength of the antisymmetric coupling. While the nonreciprocal coupling accelerates the dynamics, we can establish that time reparameterization holds exactly and is entirely governed by the equilibrium free energy landscape.

Below a critical temperature T_d, the ergodicity of the system is broken. Here, we investigate the role of time reparameterization invariance by considering the dynamics of the coupled systems at a temperature slightly above or slightly below T_d, starting from an initial configuration at infinite temperature. The fully connected nature of the model allows us to study its full time evolution in terms of spin-responses and spin–spin correlations $R_{\alpha\beta}(t,t')$ and $C_{\alpha\beta}(t,t')$, for $\alpha,\beta=1,2$. Our analysis [details in *SI Appendix*, sections 7] shows that the slow evolution of $R_{\alpha\beta}(t,t')$ and $C_{\alpha\beta}(t,t')$ is fully determined by two scalar quantities $\widetilde{C}(t,t')$, $\widetilde{R}(t,t')$, which satisfy integral equations of the form:

$$\begin{aligned}\mathcal{F}[\widetilde{C}(t,t'),\widetilde{R}(t,t')]&=0\\ \mathcal{G}[\widetilde{C}(t,t'),\widetilde{R}(t,t')]&=0,\end{aligned} \qquad [2]$$

with $\mathcal{F}$ and $\mathcal{G}$ functionals of $\widetilde{C}(t,t')$, $\widetilde{R}(t,t')$ which do not depend on γ. They are the same functionals found using equilibrium dynamics at $\gamma=0$ (50, 53). Eq. **2** determines $\widetilde{R}(t,t')$ and $\widetilde{C}(t,t')$ up to a reparameterization of time (27, 50). The choice of the specific solution of Eq. **2** is done by matching asymptotically the slow terms with the fast decaying part, whose evolution does depend on γ. The impact of γ on the slow decay of the correlations and response functions thus amounts to a time reparameterization.

The Big Picture: Franz Parisi Potential and Quasi-Dynamics

The stimulating picture emerging from our results is that both the energy landscape and the specifics of the dynamics matter. The former determines the form of the relaxation, while the latter controls the speed at which the configuration space is explored. We now provide a broader physical interpretation of the presence of time-reparameterization invariance, inspired by mean-field results.

In a given system, we introduce a notion of correlation between two configurations $\mathbf{x}$ and $\mathbf{y}$, such as

$$F_o(a,\mathbf{x},\mathbf{y})=\frac{1}{N}\sum_{i,j}\langle\theta\left(a-|\mathbf{x}_i-\mathbf{y}_j|\right)\rangle, \qquad [3]$$

where $\mathbf{x}$ is drawn from the Boltzmann distribution. We further consider the Boltzmann distribution of $\mathbf{y}$ at fixed $\mathbf{x}$, restricted to the surface $F_o(a,\mathbf{x},\mathbf{y})=q$, where q measures correlations between the two configurations. The corresponding q-dependent free energy $V(q)$ is the Franz–Parisi potential (57). A sketch of $V(q)$ for different temperatures is shown in Fig. 5 *A–C*. Within mean field, the potential is monotonic in the liquid phase and develops, at the dynamic transition point, a secondary minimum, whose location defines the Edwards-Anderson parameter q_{EA}. This minimum decreases until it becomes degenerate with the one at $q=0$ at the equilibrium transition to the glass phase.

In Fig. 5 *D–F* we sketch what would happen if we fixed *two* distances. Clearly, integrating one constraint away gives back the original one-dimensional potential. The assumption behind this picture is that, apart from the minimum at the origin, there is at most only another minimum in this potential at the position (q^1_{EA},q^2_{EA}).

Starting from here, we can make a "quasidynamic" construction step by step, as sketched in Fig. 5*G*. Very surprisingly, this construction gives, within mean field, the correct reparameterization-invariant equations for the dynamics (58, 59), just by interpreting the links in the chain as times. From this

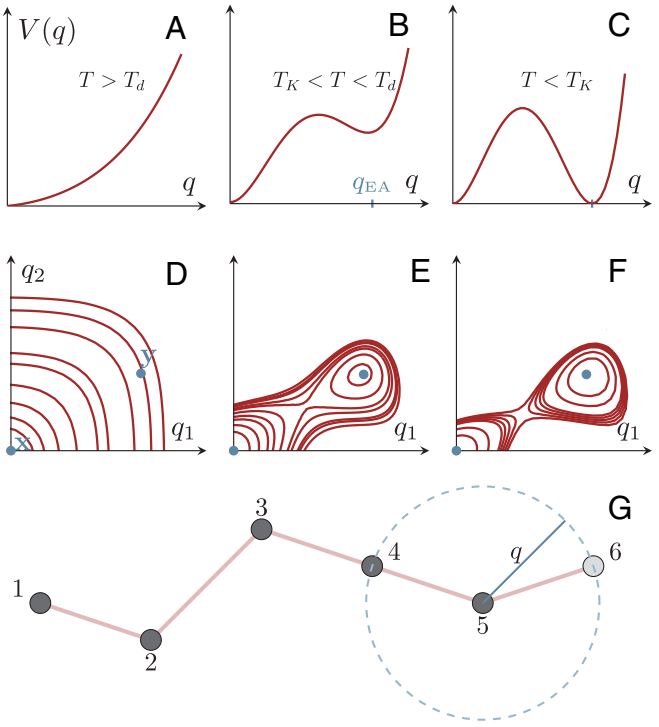

Fig. 5. Sketch of the Franz–Parisi construction in mean field: (*A*) above the dynamic transition temperature T_d. (*B*) Between the dynamic transition temperature and the static transition temperature T_K. (*C*) Below the static transition. (*D–F*) Sketch of the contour plots of a two-dimensional Franz–Parisi potential, with two "distances" q_1 and q_2 imposed. (*G*) Quasidynamics construction (58): at each step we choose a new configuration, represented by the gray circles, subject to one or more constraints, keeping all the preceding links frozen.

construction, the chain is independent of the choice of correlation used for the links. Thus, we have found a relation between correlations that is a result of a purely equilibrium calculation, as no allusion was made to an actual dynamical process. As a corollary, our numerical results in finite dimension support the existence of quasi-dynamics robust with respect to time evolution. For transverse forces and Event Chain Monte Carlo algorithm, recent analytical and numerical results substantiate the quasi-dynamics picture (40, 48): in transverse forces, odd transport significantly enhances local motion on short time-scales, but the particles eventually need to confront cage escape. In Event Chain Monte Carlo, maps of dynamical heterogeneities over long time scales have been shown to be very similar to the ones obtained with Metropolis Monte Carlo.

What we have argued in this paper is that clever algorithms work by efficiently exploiting the softness implied by time reparameterization invariance to drastically accelerate the time evolution. Numerically probing, in finite-dimensional systems, the "quasi-dynamics" picture of time-reparameterization put forth in our work is perhaps within reach, e.g. by building upon previous efforts along this direction (60–62).

Let us emphasize that the conclusion here is that the fact that different dynamical procedures leading to the same equilibrium may drastically stretch the timescales—the 'reparameterization softness'—is an observed property, one that any glass theory is required to reproduce. Even though it arises naturally in mean-field theory, it may perhaps be explained within other scenarios. It is an interesting question to understand, for instance, how this may arise, as it should, in a theory based on local elasticity.

More broadly, reparameterization softness has recently been identified as the mechanism leading to the emergence of gravity as a low-energy limit of simple quantum (SYK) models (33). Hints of time reparameterization softness have been also found in the learning dynamics of wide and deep neural networks (63). In the context of supercooled liquids, the very same mechanism underlies the drastic time-rescaling with temperature (as described by the time-temperature superposition principle), as well as under shear, aging, and barrier-crossing processes, with experimental consequences that are starting to be explored (35). We hope that the present work incentivizes the use of parametric plots as a tool to probe time reparameterization in a variety of experimental settings. In this work, we demonstrate that reparameterization softness also resolves the longstanding dichotomy between dynamical and landscape views on glasses: the latter determines reparameterization-invariant characteristics, while the former governs the actual time parameterization.

Materials and Methods

Kob–Andersen Mixture with Transverse Forces. The Kob Andersen potential is defined as (39)

$$V_{ab}(r) = 4\epsilon_{ab}\left[\left(\frac{d_{ab}}{r}\right)^{12} - \left(\frac{d_{ab}}{r}\right)^{6}\right] + C \qquad [4]$$

for $r_{ab} < 2.5d_{ab}$, and 0 otherwise. The constant C ensures that $V_{ab}(2.5d_{ab}) = 0$. The interaction diameters d_{ab} are $d_{11} = 1$ (which sets the units of length of the system), $d_{12} = d_{21} = 0.8$, $d_{22} = 0.88$, while the interaction energies ϵ_{ab} are $\epsilon_{11} = 1$ (which sets the units of energy), $\epsilon_{12} = \epsilon_{21} = 1.5$, $\epsilon_{22} = 0.5$.

The overdamped Langevin dynamics for this system is (40)

$$\dot{\mathbf{r}}_i^a = -(\mathbf{1} + \gamma\mathbf{A})\sum_{j\neq i}\sum_{b=1}^{2}\boldsymbol{\nabla}_i^a V_{ab}(|\mathbf{r}_i^a - \mathbf{r}_j^b|) + \sqrt{2T}\boldsymbol{\xi}_i^{a(t)}, \qquad [5]$$

where $\mathbf{r}_i^a$ is the position of particle i of species a, with $a = 1, 2$. $\boldsymbol{\xi}_i^a(t)$ is a Gaussian white noise with zero mean and correlations $\langle\boldsymbol{\xi}_i^a(t) \otimes \boldsymbol{\xi}_j^b(t)\rangle = \mathbf{1}\delta(t-t')\delta_{ij}\delta_{ab}$. The temperature T is measured in units of ϵ_{11}/k_B, with k_B the Boltzmann constant. The transverse forces are implemented by means of an antisymmetric matrix $\mathbf{A} = \begin{bmatrix} 0 & -1 & 0 \\ 1 & 0 & 0 \\ 0 & 0 & 0 \end{bmatrix}$ and of a dimensionless number γ that controls the amplitude of the nonequilibrium drive. When $\gamma \neq 0$, Eq. **5** is an out of equilibrium dynamics, with a steady state given by the Boltzmann distribution for the Kob–Andersen mixture. The relaxation to the stationary state for $\gamma \neq 0$ is guaranteed to be shorter than or equal to the one of equilibrium dynamics.

Simulations are performed in the NVT ensemble, using a box of side $L = 9.4d_{11}$ and a total number of particles $N_1 + N_2 = 1{,}000$, so that the number density of the system $\rho_0 = \frac{N}{V}$ is $\rho_0 \simeq 1.204$. The equations of motion given by Eq. **5** are integrated by means of the Euler–Heun algorithm using a time step $\Delta t = 10^{-4}$. The data shown are obtained from the steady-state dynamics equilibrated samples, obtained using the overdamped Langevin dynamics (Eq. **5** with $\gamma = 4$) for 10^8 time steps. The results shown in Fig. 2 of the main text are obtained by studying the stationary dynamics of 45 independent configurations.

Polydisperse Hard Spheres. The model consists of N polydisperse hard spheres in three dimensions (47). The diameters d are drawn from a power law distribution $\pi(d) \propto d^{-3}$. The boundaries of the distribution are chosen so that the polydispersity $\Delta \equiv \frac{\sqrt{\overline{d^2} - \bar{d}^2}}{\bar{d}}$ is $\Delta \approx 23\%$, with $\overline{\cdots}$ denoting an average over the diameter distribution. The average diameter $\bar{d}$ sets the units of length. The hard sphere potential between two particles i and j separated by a distance r_{ij} is defined as $V(r_{ij}) = +\infty$ if $r_{ij} < \frac{d_i + d_j}{2}$, and $V(r_{ij}) = 0$ otherwise. The simulations are done in a cubic box of linear size L with periodic boundary conditions. We explore the dynamics of the system at high packing fractions $\phi \equiv \frac{\pi}{6}\frac{N}{L^3}\overline{d^3}$.

Metropolis Algorithm. In a single timestep of the Metropolis algorithm, N Metropolis moves are performed. During a Metropolis move, a sphere is selected uniformly at random, and a displacement is proposed within a cubic box of side δ, centered around the sphere. If the displacement does not generate any overlap between the sphere and its neighbors, the move is accepted. In our simulations, we chose $\delta = 0.115$.

Event-Chain Monte Carlo. We implement the original, so called "straight" version of the Event Chain Monte Carlo algorithm (43). In the Event-Chain Monte Carlo algorithm, an activity label is assigned to a particle i chosen uniformly at random, together with a direction of motion $\mathbf{v} \in \{\mathbf{e}_x, \mathbf{e}_y\}$. The active particle is displaced along the direction $\mathbf{v}$ until a collision with another particle j occurs. After the collision, the activity label passes from particle i to particle j. The latter starts then to move along the direction $\mathbf{v}$. The iteration of this procedure produces a driven, collective displacement of a chain of particles. When the sum of the displacements of all the particles involved in the chain add up to a value ℓ, the activity label and direction of self-propulsion are uniformly resampled, initiating a new chain. One time step of the algorithm corresponds to one collision among the hard spheres, or to the random resampling of the activity label and self-propulsion direction $\mathbf{v}$. We studied the Event Chain Monte Carlo dynamics for a system of $N = 1{,}000$ polydisperse hard spheres at $\phi = 0.604$. Following (49), we chose $\ell = 0.2L$, with L the linear size of the box. The relaxation curves and the time reparameterization invariant plots for Event Chain Monte Carlo, shown in *SI Appendix*, sections 2 have been obtained by averaging over 50 independent realizations of the dynamics of the system in the steady state.

Swap Monte Carlo. In the Swap algorithm, one alternates between a set of N Metropolis moves and N swap moves. A set of N Swap moves is performed with probability p_{Swap}. During a swap move, a pair of particles is selected uniformly at random and an exchange of the particle diameters is proposed. If the exchange

does not generate overlaps with the neighbors, the move is accepted. The relaxation curves displayed in Fig. 3 of the main text and in *SI Appendix*, Fig. S4 have been obtained by averaging over 35 independent realizations of the Swap dynamics in the equilibrium state.

Collective Swap. The collective Swap algorithm implementation for a three-dimensional system of polydisperse hard spheres is described in ref. 49. We alternate randomly between a set of N Metropolis moves and a set of $N/2$ collective Swap moves. The latter set occurs with probability $p_{\mathrm{cSwap}} = 0.2$. We studied the collective Swap dynamics for s system of $N = 1{,}000$ polydisperse hard spheres at $\phi = 0.648$. The relaxation curves and the time reparameterization invariant plots, shown in *SI Appendix*, Fig. S6 are obtained by averaging over 25 independent realizations of the dynamics in the steady state.

East Model with Soft Kinetic Constraints and "Swap" Softness Updates. We consider N sites on a one dimensional, periodic lattice. Each site i has a spin value $n_i \in \{0, 1\}$ and a softness value $s_i \in \{0, 1\}$. The Hamiltonian H of the system is the one of $2N$ noninteracting spins

$$H = J\sum_i n_i + B\sum_i s_i. \qquad [6]$$

The kinetic constraints of the model are implemented by means of a constraint function C_i for each site:

$$C_i = n_{i-1} + s_i, \qquad [7]$$

which controls the rate at which a spin in site i flips. A spin n_i flips from state 1 to state 0 with rate C_i, and from state 0 to state 1 with rate $\mathrm{e}^{-J/T}$.

The softness parameter s_i can be updated in two ways (24): by means of spontaneous fluctuations or by means of "swaps" (s-updates). Spontaneous softness fluctuations take place only on site with $n_i = 1$, with rate $r_x = \mathrm{e}^{-J/T}$. When a spontaneous softness fluctuation occurs at site i the value of s_i becomes 1 or 0 with probability $(1+\mathrm{e}^{B/T})^{-1}$ or $(1+\mathrm{e}^{-B/T})^{-1}$, respectively. s-updates, on the other hand can occur on any site, independently from the value of n_i, with rate r_s, which is a parameter of the model and, when nonzero, is proportional to $\mathrm{e}^{-J/T}$. This ensures that the s-updates dynamics takes place on a similar timescale as for the creation of excitations. During an s-update, the value of the softness is updated using the same probabilities as for the spontaneous softness fluctuations.

Following (24), we fix the energy scale of the softness to $B/T = 2$. This ensures that the introduction of s-updates yields substantial speedup to the dynamics. In fact, for values of B/T too low or too big the softness and the excitation dynamics decouple, making s-updates less effective.

Since the thermodynamics of the system is the one for a system of noninteracting spins, equilibrium initial condition at a given temperature can be directly generated. The dynamics of the system is instead simulated using the Botz–Kalos–Lebowitz algorithm (64), or continuous time Monte-Carlo. In a nutshell, this is a rejection-free method that relies on computing the time that the system spends in a given configuration before transitioning to a new one, instead of proposing moves toward new configurations that are prone to rejection. At each step of the algorithm, we

1. We start from the current configuration $\mathcal{C}$ of the system at time t, given by an assignment of the spins n_i and softness s_i to the N sites.
2. Enumerate the M configurations $\mathcal{C}_1, \ldots, \mathcal{C}_M \neq \mathcal{C}$ that the system can evolve into, starting from $\mathcal{C}$, and compute the rate ω_k at which the transition $\mathcal{C} \to \mathcal{C}_k$ can happen.
3. We compute the cumulative sum $S \equiv \sum_{k=1}^{M} \omega_k$.
4. We draw a configuration $\mathcal{C}^*$ from the set of M possible configurations. The probability weight of a configuration k is ω_k/S.
5. We update the configuration $\mathcal{C}$ to the new configuration $\mathcal{C}^*$, and we increment the time by an amount $\Delta t = \frac{\log 1/r}{S}$, with r a random number uniformly distributed in the interval $(0, 1]$.
6. We update $\mathcal{C}^* \to \mathcal{C}$, $t + \Delta t \to t$ and we start back from step 1.

The data presented in the main text in Fig. 4 are the results of an average over 50 independent runs for a system of $N = 512$ sites.

***p*-Spin with Ichiki–Ohzeki Dynamics.** A p-spin spherical glass consists of N continuous spins σ_i on a fully connected lattice, interacting through a p-body Hamiltonian $H(\sigma)$. A quench disorder is introduced by means of random, coupling constants among the spins.

$$H(\sigma) \equiv \sum_{i_1<\ldots<i_p} J_{i_1\ldots i_p}\sigma_{i_1}\ldots\sigma_{i_p}. \qquad [8]$$

The coupling constants $J_{i_1\ldots i_p}$ are independent Gaussian random variable encoding the quenched disorder of the system, with variance $\overline{\left(J_{i_1\ldots i_p}\right)^2} = \frac{p!}{2N^{p-1}}$. The equilibrium overdamped Langevin dynamics for this model reads

$$\dot\sigma_i = F(\sigma_i, t) + \sqrt{2T}\xi_i(t), \qquad [9]$$

where $\xi_i(t)$ is a Gaussian white noise with correlations $\langle\xi_i(t)\xi_j(t')\rangle = 2T\delta(t-t')$. The force $F_i(\sigma_i, t) = -\frac{\partial H}{\partial\sigma_i}$ contains a contribution coming from the gradient of the Hamiltonian and a harmonic restoring force, which ensures that the spherical constraint $\sum_i\langle\sigma_i(t)^2\rangle = N$ is satisfied at all times.

The fully connected nature of the model allows to study its dynamics by means of correlations and response functions $C(t, t')$, $R(t, t')$, defined respectively as

$$\begin{aligned} R(t,t') &= \frac{1}{N}\sum_i \overline{\left\langle \frac{\partial\sigma_i(t)}{\partial h_i(t')}\Big|_{h_i=0}\right\rangle} \\ C(t,t') &= \frac{1}{N}\sum_i \overline{\langle\sigma_i(t)\sigma_i(t')\rangle}. \end{aligned} \qquad [10]$$

To illustrate the concept of time reparameterization invariance, we consider an alternative dynamics for the p-spin. It exploits the possibility of injecting a nonequilibrium drive in the system which is specifically tailored to ensure that the steady state of the system follows the Boltzmann distribution. The use of these kinds of dynamics can be rewarded by faster convergence (65). In practice, the irreversible drift is implemented by means of the so-called Ichiki–Ohzeki dynamics (66).

The nonreciprocal coupling is obtained considering two p-spin models, each having N spins $\sigma_i^{(\alpha)}$ with independent quenched disorders and a total Hamiltonian given by the sum of the Hamiltonians of the two systems, $H_{\mathrm{tot}}(\sigma^{(1)}, \sigma^{(2)}) = H(\sigma^{(1)}) + H(\sigma^{(2)})$. The two systems evolve according to an overdamped Langevin dynamics, which contains an antisymmetric coupling between the two copies:

$$\begin{bmatrix}\dot\sigma_i^{(1)}(t)\\ \dot\sigma_i^{(2)}(t)\end{bmatrix} = \begin{bmatrix}1 & -\gamma\\ \gamma & 1\end{bmatrix}\begin{bmatrix}F^{(1)}(\sigma_i^{(1)}, t)\\ F^{(2)}(\sigma_i^{(2)}, t)\end{bmatrix} + \begin{bmatrix}\sqrt{2T}\xi_i^{(1)}(t)\\ \sqrt{2T}\xi_i^{(2)}(t)\end{bmatrix}. \qquad [11]$$

The realization of the Gaussian noises $\xi_i^{(\alpha)}(t)$ are independent from one system to the other. The parameter γ encodes the strength of the nonreciprocal forces exerted between the two copies. For $\gamma = 0$, we fall back to the case of two independent p-spin models evolving through an equilibrium dynamics. When $\gamma \neq 0$, the dynamics becomes out of equilibrium, but it admits the Boltzmann distribution $\rho_{\mathrm{B}} \propto \mathrm{e}^{-\beta H_{\mathrm{tot}}}$ in its steady state, which is reached with a shorter relaxation time compared to the equilibrium case (56).

The steady-state dynamics of Eq. **11** has been studied previously (56), quantifying the acceleration of the system in an ergodic region above T_d, the dynamical transition temperature below ergodicity is broken. T_d is the same as in equilibrium. Below a critical temperature T_d, the ergodicity of the system is broken. Here, we investigate the role of time reparameterization invariance by considering the dynamics of the coupled systems at temperature slightly above or slightly below T_d, starting from an initial configuration at infinite temperature. We consider a generalization of Eq. **10** to encode responses and correlations internal to each copy and among each copy of the system in two 2×2 matrices $R_{\alpha\beta}(t, t')$ and $C_{\alpha\beta}(t, t')$. From this quantities, which encode the full time evolution of the system, we isolate a slow contribution $\widetilde{C}_{\alpha\beta}(t, t')$,

$\widetilde{R}_{\alpha\beta}(t,t')$, for which $\partial_t \widetilde{C}_{\alpha\beta}(t,t') \approx \partial_t \widetilde{R}_{\alpha\beta}(t,t') \approx 0$. Imposing the *ansatz* $C_{\alpha\beta} = \delta_{\alpha\beta}\widetilde{C}(t,t')$, $\widetilde{R}_{\alpha\beta} = \frac{1}{1+\gamma^2}\widetilde{R}(t,t')(\delta_{\alpha\beta} + \gamma\epsilon_{\alpha\beta})$, with $\epsilon_{\alpha\beta}$ the Levi-Civita tensor, we obtain the pair of integral equations

$$
\begin{aligned}
0 &= \left[-\frac{T}{1-q} + \frac{p(p-1)}{2T}(1-q)\widetilde{C}(t,t')^{p-2}\right]\widetilde{R}(t,t') \\
&\quad + \frac{p(p-1)}{2}\int_{t'}^{t} \mathrm{d}\tau \widetilde{C}(t,\tau)^{p-2}\widetilde{R}(t,\tau)\widetilde{R}(\tau,t') \\
0 &= \left[-\frac{T}{1-q} + \frac{p}{2T}(1-q)\widetilde{C}(t,t')^{p-2}\right]\widetilde{C}(t,t') \\
&\quad + \frac{p}{2}\int_{t'}^{t} \mathrm{d}\tau \widetilde{C}(t,t')^{p-1}\widetilde{R}(\tau,t') \\
&\quad + \frac{p(p-1)}{2}\int_{0}^{t} \mathrm{d}\tau \widetilde{C}(t,\tau)^{p-2}\widetilde{R}(t,\tau)\widetilde{C}(\tau,t'). \qquad \textbf{[12]}
\end{aligned}
$$

If $T > T_d$, the quantity q is the height of the transient, long-lived plateau crossed by the correlation function during the relaxation process. If $T \leq T_d$, q is the Edwards-Anderson order parameter (67), which can be determined from the thermodynamics of the system. More details about the derivation can be found in *SI Appendix*, sections 7. These equations define explicitly the functionals $\mathcal{F}$ and $\mathcal{G}$ introduced in Eq. **2**.

Data, Materials, and Software Availability. The data used to produce the figures in this paper are publicly available in a Github repository (68).

ACKNOWLEDGMENTS. We warmly acknowledge very useful discussions with Rob Jack, Juan P. Garrahan, Giorgio Parisi, and Pierfrancesco Urbani. F.G., L.B., and F.v.W. acknowledge the financial support of the French Agence Nationale de la Recherche (ANR) through the project Thermodynamics of Active Matter, under the grant ANR THEMA No. 20-CE30-0031-01. F.G. acknowledges support from Stanford's Leinweber Institute of Theoretical Physics.

Author affiliations: [a]Laboratoire Matière et Systèmes Complexes, Université Paris Cité & CNRS (UMR 7057), Paris 75013, France; [b]Department of Applied Physics, Stanford University, Stanford, CA 94305; [c]Laboratoire Charles Coulomb, Université de Montpellier & CNRS (UMR 5221), Montpellier 34095, France; [d]Gulliver, UMR CNRS 7083, École supérieure de physique et de chimie industrielles Paris, Université Paris Sciences et Lettres Research University, Paris 75005, France; and [e]Laboratoire de Physique de l'École Normale Supérieure, École Normale Supérieure, Paris 75005, France

1. C. P. Royall *et al.*, Colloidal hard spheres: Triumphs, challenges, and mysteries. *Rev. Mod. Phys.* **96**, 045003 (2024).
2. J. P. Bouchaud, Why is the dynamics of glasses super-Arrhenius? arXiv [Preprint] (2024). http://arxiv.org/abs/2402 01883 (Accessed 6 January 2026).
3. G. Parisi, P. Urbani, F. Zamponi, *Theory of Simple Glasses* (Cambridge University Press, 2020).
4. T. Maimbourg, J. Kurchan, F. Zamponi, Solution of the dynamics of liquids in the large-dimensional limit. *Phys. Rev. Lett.* **116**, 015902 (2016).
5. G. Adam, J. H. Gibbs, On the temperature dependence of cooperative relaxation properties in glass-forming liquids. *J. Chem. Phys.* **43**, 139–146 (1965).
6. M. Goldstein, Viscous liquids and the glass transition: A potential energy barrier picture. *J. Chem. Phys.* **51**, 3728–3739 (1969).
7. F. H. Stillinger, T. A. Weber, Hidden structure in liquids. *Phys. Rev. A* **25**, 978 (1982).
8. F. H. Stillinger, A topographic view of supercooled liquids and glass formation. *Science* **267**, 1935–1939 (1995).
9. C. Angell, "Entropy, fragility, "landscapes", and the glass transition" in *Complex Behaviour of Glassy Systems: Proceedings of the XIV Sitges Conference Sitges, Barcelona, Spain, 10–14 June 1996*, M. Rubí, C. Pérez-Vicente, Eds. (Springer, 2007), pp. 1–21.
10. F. H. Stillinger, *Energy Landscapes, Inherent Structures, and Condensed-Matter Phenomena* (Princeton University Press, 2015).
11. J. P. Bouchaud, G. Biroli, On the Adam-Gibbs-Kirkpatrick-Thirumalai-Wolynes scenario for the viscosity increase in glasses. *J. Chem. Phys.* **121**, 7347–7354 (2004).
12. G. Biroli, J. P. Bouchaud, Diverging length scale and upper critical dimension in the Mode-Coupling theory of the glass transition. *Europhys. Lett.* **67**, 21 (2004).
13. A. Montanari, G. Semerjian, Rigorous inequalities between length and time scales in glassy systems. *J. Stat. Phys.* **125**, 23–54 (2006).
14. G. Biroli, J. P. Bouchaud, A. Cavagna, T. S. Grigera, P. Verrocchio, Thermodynamic signature of growing amorphous order in glass-forming liquids. *Nat. Phys.* **4**, 771–775 (2008).
15. J. Kurchan, D. Levine, Correlation length for amorphous systems. arXiv [Preprint] (2009). http://arxiv.org/abs/0904.4850 (Accessed 6 January 2026).
16. J. Kurchan, D. Levine, Order in glassy systems. *J. Phys. A Math. Theor.* **44**, 035001 (2010).
17. A. S. Keys, L. O. Hedges, J. P. Garrahan, S. C. Glotzer, D. Chandler, Excitations are localized and relaxation is hierarchical in glass-forming liquids. *Phys. Rev. X* **1**, 021013 (2011).
18. F. Ritort, P. Sollich, Glassy dynamics of kinetically constrained models. *Adv. Phys.* **52**, 219–342 (2003).
19. M. Wyart, M. E. Cates, Does a growing static length scale control the glass transition? *Phys. Rev. Lett.* **119**, 195501 (2017).
20. L. Berthier, G. Biroli, J. P. Bouchaud, G. Tarjus, Can the glass transition be explained without a growing static length scale? *J. Chem. Phys.* **150**, 094501 (2019).
21. T. S. Grigera, G. Parisi, Fast Monte Carlo algorithm for supercooled soft spheres. *Phys. Rev. E* **63**, 045102 (2001).
22. A. Ninarello, L. Berthier, D. Coslovich, Models and algorithms for the next generation of glass transition studies. *Phys. Rev. X* **7**, 021039 (2017).
23. L. Berthier *et al.*, Configurational entropy measurements in extremely supercooled liquids that break the glass ceiling. *Proc. Natl. Acad. Sci. U.S.A.* **114**, 11356–11361 (2017).
24. R. Gutiérrez, J. P. Garrahan, R. L. Jack, Accelerated relaxation and suppressed dynamic heterogeneity in a kinetically constrained (East) model with swaps. *J. Stat. Mech. Theory Exp.* **2019**, 094006 (2019).
25. G. Alfaro Miranda, L. F. Cugliandolo, M. Tarzia, SWAP algorithm for lattice spin models. *Phys. Rev. E* **110**, L043301 (2024).
26. H. Sompolinsky, A. Zippelius, Relaxational dynamics of the Edwards-Anderson model and the mean-field theory of spin-glasses. *Phys. Rev. B* **25**, 6860–6875 (1982).
27. C. Chamon, M. P. Kennett, H. E. Castillo, L. F. Cugliandolo, Separation of time scales and reparametrization invariance for aging systems. *Phys. Rev. Lett.* **89**, 217201 (2002).
28. C. Chamon, P. Charbonneau, L. F. Cugliandolo, D. R. Reichman, M. Sellitto, Out-of-equilibrium dynamical fluctuations in glassy systems. *J. Chem. Phys.* **121**, 10120–10137 (2004).
29. C. Chamon, L. F. Cugliandolo, Fluctuations in glassy systems. *J. Stat. Mech.* **2007**, P07022 (2007).
30. K. E. Avila, H. E. Castillo, A. Parsaeian, Fluctuations in the time variable and dynamical heterogeneity in glass-forming systems. *Phys. Rev. E* **88**, 042311 (2013).
31. H. E. Castillo, A. Parsaeian, Local fluctuations in the ageing of a simple structural glass. *Nat. Phys.* **3**, 26–28 (2007).
32. A. Kitaev, A simple model of quantum holography (2015). https://online.kitp.ucsb.edu/online/entangled15/kitaev2/.
33. J. Maldacena, D. Stanford, Remarks on the Sachdev-Ye-Kitaev model. *Phys. Rev. D* **94**, 106002 (2016).
34. T. Rizzo, Path integral approach unveils role of complex energy landscape for activated dynamics of glassy systems. *Phys. Rev. B* **104**, 094203 (2021).
35. T. Böhmer *et al.*, Time reversibility during the ageing of materials. *Nat. Phys.* **20**, 637–645 (2024).
36. I. M. Douglass, J. C. Dyre, Distance-as-time in physical aging. *Phys. Rev. E* **106**, 054615 (2022).
37. B. Riechers *et al.*, Predicting nonlinear physical aging of glasses from equilibrium relaxation via the material time. *Sci. Adv.* **8**, eabl9809 (2022).
38. J. C. Dyre, Perspective: Excess-entropy scaling. *J. Chem. Phys.* **149**, 210901 (2018).
39. W. Kob, H. C. Andersen, Scaling behavior in the β-relaxation regime of a supercooled Lennard-Jones mixture. *Phys. Rev. Lett.* **73**, 1376 (1994).
40. F. Ghimenti, L. Berthier, G. Szamel, F. van Wijland, Sampling efficiency of transverse forces in dense liquids. *Phys. Rev. Lett.* **131**, 257101 (2023).
41. F. Ghimenti, L. Berthier, G. Szamel, F. van Wijland, Transverse forces and glassy liquids in infinite dimensions. *Phys. Rev. E* **109**, 064133 (2024).
42. F. Ghimenti, L. Berthier, G. Szamel, F. van Wijland, Irreversible Boltzmann samplers in dense liquids: Weak-coupling approximation and mode-coupling theory. *Phys. Rev. E* **110**, 034604 (2024).
43. E. P. Bernard, W. Krauth, D. B. Wilson, Event-chain Monte Carlo algorithms for hard-sphere systems. *Phys. Rev. E* **80**, 056704 (2009).
44. H. Ikeda, F. Zamponi, A. Ikeda, Mean field theory of the swap Monte Carlo algorithm. *J. Chem. Phys.* **147**, 234506 (2017).
45. G. Szamel, Theory for the dynamics of glassy mixtures with particle size swaps. *Phys. Rev. E* **98**, 050601 (2018).
46. C. Brito, E. Lerner, M. Wyart, Theory for swap acceleration near the glass and jamming transitions for continuously polydisperse particles. *Phys. Rev. X* **8**, 031050 (2018).
47. L. Berthier, D. Coslovich, A. Ninarello, M. Ozawa, Equilibrium sampling of hard spheres up to the jamming density and beyond. *Phys. Rev. Lett.* **116**, 238002 (2016).
48. F. Ghimenti, L. Berthier, F. van Wijland, Irreversible Monte Carlo algorithms for hard disk glasses: From event-chain to collective swaps. *Phys. Rev. Lett.* **133**, 028202 (2024).
49. L. Berthier, F. Ghimenti, F. van Wijland, Monte Carlo simulations of glass-forming liquids beyond metropolis. *J. Chem. Phys.* **161**, 114105 (2024).
50. L. F. Cugliandolo, J. Kurchan, Weak ergodicity breaking in mean-field spin-glass models. *Philos. Mag. B* **71**, 501–514 (1995).
51. L. F. Cugliandolo, J. Kurchan, On the out-of-equilibrium relaxation of the Sherrington-Kirkpatrick model. *J. Phys. A Math. Gen.* **27**, 5749 (1994).
52. S. Mehri, L. Costigliola, J. C. Dyre, Single-parameter aging in the weakly nonlinear limit. *Thermo* **2**, 160–170 (2022).
53. L. F. Cugliandolo, J. Kurchan, Analytical solution of the off-equilibrium dynamics of a long-range spin-glass model. *Phys. Rev. Lett.* **71**, 173 (1993).
54. L. F. Cugliandolo, J. Kurchan, L. Peliti, Energy flow, partial equilibration, and effective temperatures in systems with slow dynamics. *Phys. Rev. E* **55**, 3898 (1997).
55. L. F. Cugliandolo, The effective temperature. *J. Phys. A Math. Theor.* **44**, 483001 (2011).
56. F. Ghimenti, F. van Wijland, Accelerating, to some extent, the *p*-spin dynamics. *Phys. Rev. E* **105**, 054137 (2022).

57. S. Franz, G. Parisi, Phase diagram of coupled glassy systems: A mean-field study. *Phys. Rev. Lett.* **79**, 2486–2489 (1997).
58. S. Franz, G. Parisi, Quasi-equilibrium in glassy dynamics: An algebraic view. *J. Stat. Mech. Theory Exp.* **2013**, P02003 (2013).
59. S. Franz, G. Parisi, P. Urbani, Quasi-equilibrium in glassy dynamics: A liquid theory approach. *J. Phys. A Math. Theor.* **48**, 19FT01 (2015).
60. J. M. Bomont, J. P. Hansen, G. Pastore, An investigation of the liquid to glass transition using integral equations for the pair structure of coupled replicae. *J. Chem. Phys.* **141**, 174505 (2014).
61. J. M. Bomont, J. P. Hansen, G. Pastore, Revisiting the replica theory of the liquid to ideal glass transition. *J. Chem. Phys.* **150**, 154504 (2019).
62. B. Guiselin, G. Tarjus, L. Berthier, On the overlap between configurations in glassy liquids. *J. Chem. Phys.* **153**, 224502 (2020).
63. A. Atanasov, A. Meterez, J. B. Simon, C. Pehlevan, The optimization landscape of sgd across the feature learning strength. arXiv [Preprint] (2024). http://arxiv.org/abs/2410.04642 (Accessed 6 January 2026).
64. A. B. Bortz, M. H. Kalos, J. L. Lebowitz, A new algorithm for Monte Carlo simulation of Ising spin systems. *J. Comput. Phys.* **17**, 10–18 (1975).
65. C. R. Hwang, S. Y. Hwang-Ma, S. J. Sheu, Accelerating Gaussian diffusions. *Ann. Appl. Probab.* **3**, 897–913 (1993).
66. M. Ohzeki, A. Ichiki, Langevin dynamics neglecting detailed balance condition. *Phys. Rev. E* **92**, 012105 (2015).
67. S. F. Edwards, P. W. Anderson, Theory of spin glasses. *J. Phys. F Metal Phys.* **5**, 965 (1975).
68. F. Ghimenti, L. Berthier, J. Kurchan, F. van Wijland, Data from "Clever algorithms for glasses work by time reparametrization." GitHub. https://github.com/FedericoGhimenti/CleverAlgorithmsTimeReparametrization. Deposited 6 January 2026.